Inhibitory Plasticity Balances Excitation and Inhibition in Sensory Pathways and Memory Networks

T. P. Vogels, *et al.*

Science **334**, 1569 (2011);
DOI: 10.1126/science.1211095

Science (print ISSN 0036-8075; online ISSN 1095-9203) is published weekly, except the last week in December, by the American Association for the Advancement of Science, 1200 New York Avenue NW, Washington, DC 20005.

pronounced than in *drbp* nulls (*5*, *14*). Functionally, *drbp* and *bruchpilot* phenotypes appear similar: Both demonstrate decreased and desynchronized evoked SV release with atypical short-term facilitation. However, the deficits in evoked SV release are much more severe in *drbp* nulls than in *bruchpilot* nulls [i.e., release occurs at 5% versus 30% (*5*) of the respective wild-type level]. DRBP levels were clearly reduced in *bruchpilot* mutants (fig. S7), whereas gross Bruchpilot levels were not altered in *drbp* mutants (Fig. 2B). Given that even a partial loss of DRBP causes marked reduction in SV release (Fig. 3A), deficits in *bruchpilot* mutants might be explained, at least in part, by a concomitant loss of DRBP, and DRBP probably serves functions beyond the structural and Ca^{2+} channel–clustering roles of Bruchpilot.

Taken together, we identified DRBP as a central part of the AZ cytomatrix. How, in detail, DRBP functionally integrates into this protein network is subject to future analyses. Notably, the short-term plasticity phenotype of *drbp* mutants is reminiscent of mammalian *munc13-1* KO and *caps-1* and *caps-2* DKO mutants (*25*, *26*), which implicates functional links between priming factors and DRBP. Consistent with the functional importance of the DRBP protein family suggested by our study, human genetics recently identified two *rbp* loci associated with autism with high confidence (*27*, *28*).

References and Notes

1. Y. Jin, C. C. Garner, *Annu. Rev. Cell Dev. Biol.* **24**, 237 (2008).
2. S. J. Sigrist, D. Schmitz, *Curr. Opin. Neurobiol.* **21**, 144 (2011).
3. S. Schoch, E. D. Gundelfinger, *Cell Tissue Res.* **326**, 379 (2006).
4. L. Siksou, A. Triller, S. Marty, *Curr. Opin. Neurobiol.* **21**, 261 (2011).
5. R. J. Kittel *et al.*, *Science* **312**, 1051 (2006).
6. Y. Wang, S. Sugita, T. C. Sudhof, *J. Biol. Chem.* **275**, 20033 (2000).
7. H. Hibino *et al.*, *Neuron* **34**, 411 (2002).
8. S. A. Spangler, C. C. Hoogenraad, *Biochem. Soc. Trans.* **35**, 1278 (2007).
9. T. Mittelstaedt, S. Schoch, *Gene* **403**, 70 (2007).
10. S. W. Hell, *Science* **316**, 1153 (2007).
11. J. Bückers, D. Wildanger, G. Vicidomini, L. Kastrup, S. W. Hell, *Opt. Express* **19**, 3130 (2011).
12. J. Hou, T. Tamura, Y. Kidokoro, *J. Neurophysiol.* **100**, 2833 (2008).
13. F. Kawasaki, R. Felling, R. W. Ordway, *J. Neurosci.* **20**, 4885 (2000).
14. W. Fouquet *et al.*, *J. Cell Biol.* **186**, 129 (2009).
15. F. Kawasaki, S. C. Collins, R. W. Ordway, *J. Neurosci.* **22**, 5856 (2002).
16. K. J. Venken, Y. He, R. A. Hoskins, H. J. Bellen, *Science* **314**, 1747 (2006).
17. L. Siksou *et al.*, *J. Neurosci.* **27**, 6868 (2007).
18. P. Rostaing, R. M. Weimer, E. M. Jorgensen, A. Triller, J. L. Bessereau, *J. Histochem. Cytochem.* **52**, 1 (2004).
19. S. Hallermann *et al.*, *J. Neurosci.* **30**, 14340 (2010).
20. E. O. Gracheva, E. B. Maryon, M. Berthelot-Grosjean, J. E. Richmond, *Front. Synaptic Neurosci.* **2**, 141 (2010).
21. E. Neher, T. Sakaba, *Neuron* **59**, 861 (2008).
22. F. Kawasaki, B. Zou, X. Xu, R. W. Ordway, *J. Neurosci.* **24**, 282 (2004).
23. P. S. Kaeser *et al.*, *Cell* **144**, 282 (2011).
24. Y. Han, P. S. Kaeser, T. C. Südhof, R. Schneggenburger, *Neuron* **69**, 304 (2011).
25. C. Rosenmund *et al.*, *Neuron* **33**, 411 (2002).
26. W. J. Jockusch *et al.*, *Cell* **131**, 796 (2007).
27. M. Bucan *et al.*, *PLoS Genet.* **5**, e1000536 (2009).
28. D. Pinto *et al.*, *Nature* **466**, 368 (2010).

Acknowledgments: This work was supported by Deutsche Forschungsgemeinschaft (DFG) grants (SFB 665, SFB 958, and EXC 257) to S.J.S and D.S., as well as Bundesministerium für Bildung und Forschung (The German Federal Agency of Education and Research) funding for Deutsche Zentrum für Neurodegenerative Erkrankungen (DZNE) to D.S. Also, M.S. was supported by a Ph.D. fellowship from the Max Delbrück Center for Molecular Medicine and a Boehringer Ingelheim Fonds Ph.D. fellowship. E.K. and S.W. were supported by Ph.D. fellowships from the graduate school GRK 1123 funded by the DFG. M.M. was supported by a fellowship of the Swiss National Science Foundation (PBSKP3-123456/1).

Supporting Online Material

www.sciencemag.org/cgi/content/full/334/6062/1565/DC1
Materials and Methods
Figs. S1 to S7
References (*29*–*39*)

22 August 2011; accepted 2 November 2011
10.1126/science.1212991

Inhibitory Plasticity Balances Excitation and Inhibition in Sensory Pathways and Memory Networks

T. P. Vogels,[1]*† H. Sprekeler,[1]* F. Zenke,[1] C. Clopath,[1,2] W. Gerstner[1]

Cortical neurons receive balanced excitatory and inhibitory synaptic currents. Such a balance could be established and maintained in an experience-dependent manner by synaptic plasticity at inhibitory synapses. We show that this mechanism provides an explanation for the sparse firing patterns observed in response to natural stimuli and fits well with a recently observed interaction of excitatory and inhibitory receptive field plasticity. The introduction of inhibitory plasticity in suitable recurrent networks provides a homeostatic mechanism that leads to asynchronous irregular network states. Further, it can accommodate synaptic memories with activity patterns that become indiscernible from the background state but can be reactivated by external stimuli. Our results suggest an essential role of inhibitory plasticity in the formation and maintenance of functional cortical circuitry.

The balance of excitatory and inhibitory membrane currents that a neuron experiences during stimulated and ongoing activity has been the topic of many studies (*1*–*11*). This balance, first defined as equal average amounts of de- and hyperpolarizing membrane currents (from here on referred to as "global balance"), is essential for maintaining stability of cortical networks (*1*, *2*). Balanced networks display asynchronous irregular (AI) dynamics that mimic activity patterns observed in cortical neurons. Such asynchronous network states facilitate rapid responses to small changes in the input (*2*, *3*, *12*), providing an ideal substrate for cortical signal processing (*4*, *13*, *14*).

Moreover, input currents to cortical neurons are not merely globally balanced but also coupled in time (*5*, *6*, *15*) and cotuned for different stimulus features (*7*, *8*). The tight coupling of excitation and inhibition suggests a more precise, detailed balance, in which each excitatory input arrives at the cell together with an inhibitory counterpart (Fig. 1A), permitting sensory inputs to be transiently (*9*) or persistently turned on by targeted disruptions of the balance (*10*, *11*).

Although the excitatory-inhibitory balance plays an important role for stability and information processing in cortical networks, it is not understood by which mechanisms this balance is established and maintained during ongoing sensory experiences. Inspired by recent experimental results (*7*), we investigated the hypothesis that synaptic plasticity at inhibitory synapses plays a central role in balancing the excitatory and inhibitory inputs a cell receives.

We simulated a single postsynaptic integrate-and-fire neuron receiving correlated excitatory and inhibitory input signals. The cell received input through 1000 synapses (Fig. 1B), which were divided into eight independent groups of 100 excitatory and 25 inhibitory synapses. All excitatory and inhibitory synapses within each group followed the same temporally modulated rate signal (time constant $\tau \sim 50$ ms) to mimic ongoing sensory activity (*13*, *16*). Spikes were generated from independent Poisson processes, leading to 125 different spike trains per signal. This architecture allowed each signal to reach the cell simultaneously through both excitatory and inhibitory synapses (Fig. 1B). To mimic glutamatergic and γ-aminobutyric acid (GABAergic) transmission, the synapses were conductance-based

[1]School of Computer and Communication Sciences and Brain-Mind Institute, École Polytechnique Fédérale de Lausanne, 1015 Lausanne EPFL, Switzerland. [2]CNRS, UMR 8119, Université Paris Descartes, 45 Rue des Saints Pères, 75270 Paris Cedex 06, France.

*These authors contributed equally to this work.
†To whom correspondence should be addressed. E-mail: tim.vogels@epfl.ch

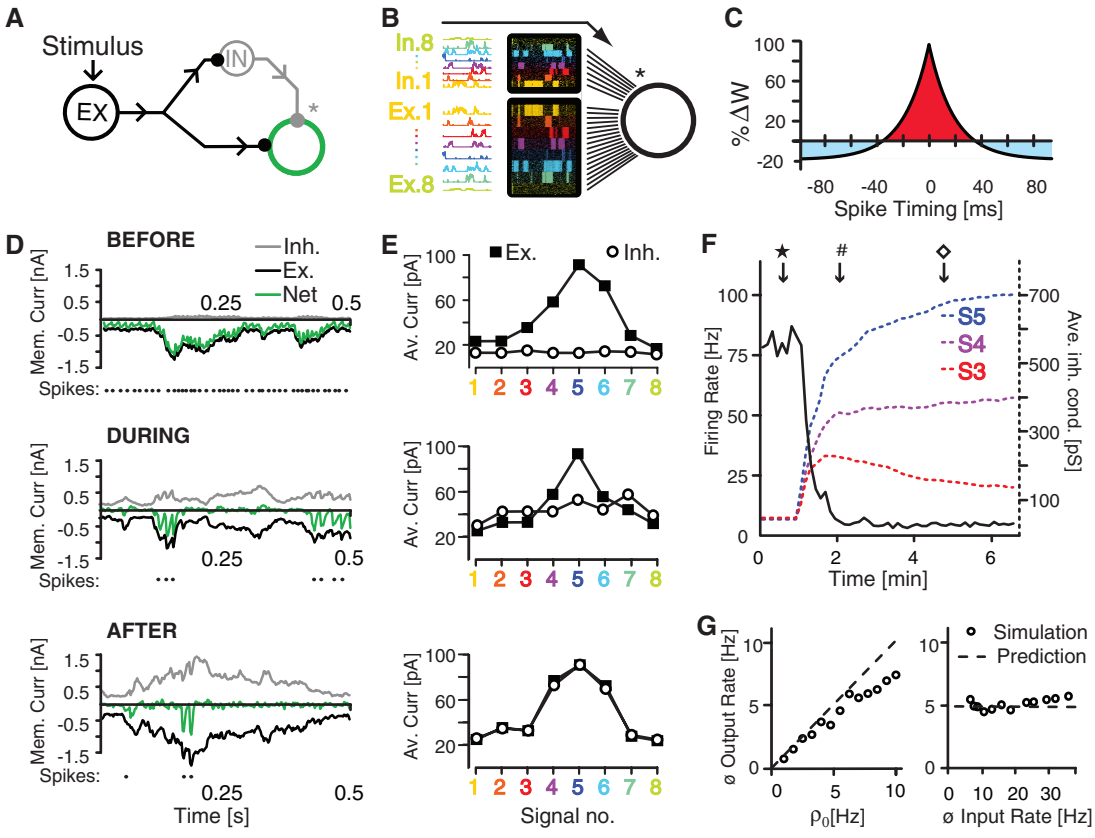

Fig. 1. Inhibitory synaptic plasticity balances excitation and inhibition. (**A**) Feedforward inhibition: Excitatory input reaches a target region through both direct excitation and indirect disynaptic inhibition. (**B**) Feedforward inhibition for a single postsynaptic cell: Eight groups of 100 excitatory and 25 inhibitory synapses each deliver spikes to a single postsynaptic cell. Spiking probabilities are homogeneous within the groups but vary in time, simulating eight separate (color-coded) signal channels that reach the cell simultaneously through excitatory and inhibitory synapses. (**C**) Spike-timing–dependent learning rule: Near-coincident pre- and postsynaptic spikes potentiate inhibitory synapses [marked with * in (A) and (B)], whereas every presynaptic spike causes synaptic depression. (**D**) Total excitatory (black), inhibitory (gray), and net (green) membrane currents before, during, and after inhibitory synaptic plasticity. The resulting spikes are indicated as dots underneath each current plot. (**E**) Excitatory and inhibitory membrane currents (black and white symbols, respectively) evoked by each signal channel, averaged over 4 s, before, during, and after inhibitory synaptic plasticity (top, middle, and bottom, respectively). (**F**) Temporal evolution of the postsynaptic firing rate (solid line) and the average synaptic weights of the inhibitory synapses associated with three representative signals (dotted lines). ★, #, and ◊ indicate the times at which the top, middle, and bottom graphs of (D) and (E) were recorded. (**G**) Average firing rate of the postsynaptic neuron after learning, plotted for different values of target firing rate ρ_0 (left) and different input rates (right). The dashed lines in both graphs show the analytical predictions.

with reversal potentials $V^E = 0$ mV and $V^I = -80$ mV and time constants $\tau^E = 5$ ms, and $\tau^I = 10$ ms for excitation and inhibition, respectively [see supporting online material (SOM)]. The strength of the inhibitory synapses was initially weak but could change according to a spike-timing–dependent plasticity rule, in which near-coincident pre- and postsynaptic spikes induce potentiation of the synapse (*17*–*19*). Additionally, every presynaptic spike leads to synaptic depression (*17*, *18*) (Fig. 1C). This learning rule can be summarized as

$$\Delta w = \eta(pre \times post - \rho_0 \times pre) \qquad (1)$$

where Δw denotes the change in synaptic efficacy, *pre* and *post* are the pre- and postsynaptic activity, η is the learning rate, and ρ_0 is a constant that acts as a target rate for the postsynaptic neuron (see SOM Sec. 2 for a mathematical analysis).

Whereas inhibitory synapses were plastic, the efficacies of the excitatory model synapses were fixed at the beginning of a simulation and left unchanged unless otherwise noted. Analogous to frequency- or orientation-tuned sensory neurons, excitatory synapses were tuned to have a preferred signal (Fig. 1E). Because all excitatory synapses were set to nonzero strengths, the postsynaptic neuron fired at high rates when the inhibitory synapses were weak at the beginning of a simulation (Fig. 1, D and E, top, and F). The resulting high number of pairs of pre- and postsynaptic spikes led to relatively indiscriminate strengthening of all inhibitory synapses (Fig. 1, D and E, middle) until excitatory and inhibitory membrane currents became approximately balanced and the postsynaptic firing rate was dramatically reduced (Fig. 1F). In this globally balanced state, only unbalanced excitatory signals led to coincident pairs of pre- and postsynaptic spikes, consequently strengthening underpowered inhibitory synapses. Those inhibitory synapses that were stronger than their excitatory counterparts kept the postsynaptic side unresponsive and were thus weakened (because of sole presynaptic firing) until they allowed postsynaptic spiking again. Over time, this led to a precise, detailed balance of excitatory and inhibitory synaptic weights for each channel (Fig. 1, D and E, bottom). In agreement with the mathematical analysis, the postsynaptic firing rate was determined mainly by the depression factor, ρ_0, but not by the average input firing rate to the postsynaptic neuron (Fig. 1G). The mechanism was robust to plausible delays of several milliseconds. However, because detailed balance requires a correlation between excitatory and inhibitory synaptic inputs, the balance deteriorated when the delay between excitation and inhibition increased to values larger than the autocorrelation time of the input signals and the coincidence time of the Hebbian learning rule, but global balance still persisted (fig. S2).

To investigate how the state of the balance affects the neuron's response properties, we presented a fixed stimulus sequence to the neuron (Fig. 2A) and compared the spiking response over 50 trials to the input rates of each signal. In the globally balanced state (Fig. 2B, top) in which inhibitory synapses were distributed so that excitation and inhibition were balanced only on average across all channels, the peristimulus time histogram (PSTH) faithfully reproduced the firing rates of the preferred signals. The other, non-preferred input signals evoked more inhibition than excitation and thus had no impact on the cell's firing behavior. An additional steplike input rate protocol, in which 100-ms-long pulses of various step sizes (Fig. 2C) were presented to one channel at a time, revealed that spiking responses are largely insensitive to stimulus intensity and indeed narrowly tuned to the preferred stimulus, giving rise to an all-or-none response (Fig. 2, D and E).

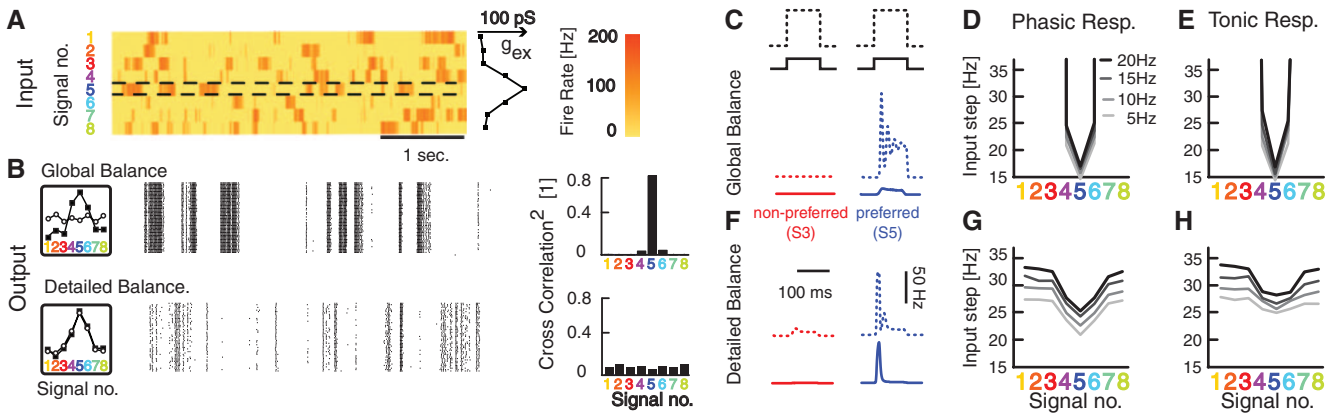

Fig. 2. Inhibitory synaptic plasticity sparsifies and democratizes receptive fields. (**A**) A fixed sequence of eight stimuli of varying firing rates is fed repetitively into a postsynaptic cell. Excitatory synapses are strength-tuned by signal group (see conductance graph on the right) so that signal five (marked also by dashed lines) is the preferred signal. (**B**) Postsynaptic spikes over 50 trials with globally or detailed balanced inhibitory synapses (top and bottom graphs, respectively) as indicated by the schematics on the left (compare with Fig. 1E). The normalized and squared cross-correlation coefficients between each input signal and the PSTH are also shown (right). (**C**) Schematic of a step stimulus delivered with large and small step sizes (solid and dotted black lines respectively); Sample PSTHs for nonpreferred (red) and preferred (blue) stimuli to both step sizes are shown for a globally balanced cell. (**D** and **E**) Iso-response contour lines of the postsynaptic cell in the globally balanced regime during the onset (phasic) (0 to 50 ms) (D) and tonic (50 to 100 ms) (E) parts of the response. (**F**) Sample responses for nonpreferred (red) and preferred (blue) stimuli to both step stimuli [as in (C)]. (**G** and **H**) Iso-response contour lines [as in (D) and (E)] for a detailed balanced cell.

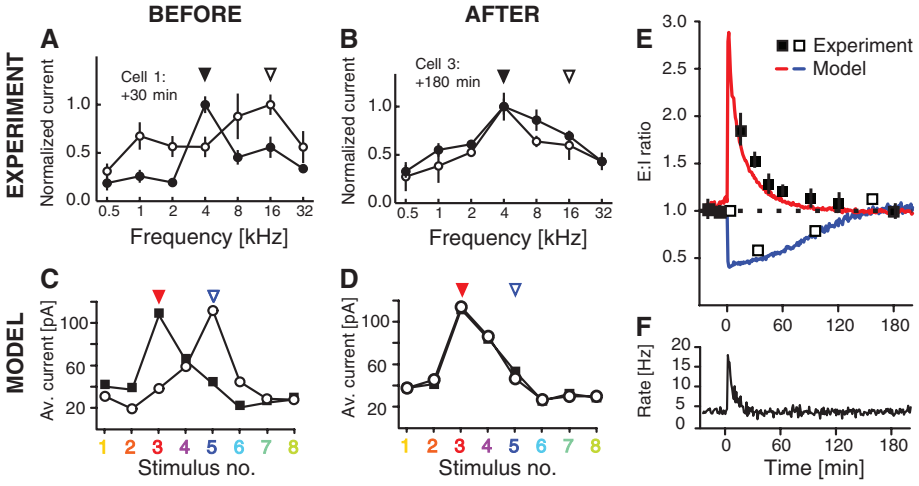

Fig. 3. Temporal dynamics of inhibitory plasticity, experiment, and model. Frequency-tuned excitatory and inhibitory membrane currents (black and white symbols, respectively) as recorded from pyramidal cells in the primary auditory cortex of adult rat (*7*) (**A**) 30 min and (**B**) 180 min after a stimulus protocol shifted the preferred frequency of the excitatory membrane currents from 16 to 4 kHz. Similarly stimulus-tuned input currents in a simulation (**C**) 30 min and (**D**) 180 min after (manually) changing the excitatory tuning curve. Solid and open arrowheads indicate the previous and the new preferred stimuli in all panels. (**E**) Summary plot of the ratios of excitatory and inhibitory current amplitudes of previously preferred stimuli and new preferred stimuli, as indicated in (A) to (D), in the experiment (open and solid symbols, respectively) and simulations (blue and red lines, respectively). (**F**) Firing rate of the simulated neuron over the time of the simulation in (E). Error bars indicate SEM. [(A), (B), and (E) adapted from (*7*) with permission]

In the detailed balanced state, the response of the cell was sparse (Fig. 2B, bottom) and reminiscent of experimental observations (*16*, *20*–*22*) across many sensory systems. Spikes were caused primarily by transients in the input signals, during which the faster dynamics of the excitatory synapses momentarily overcame inhibition. Sustained episodes of presynaptic firing, on the other hand, caused steady membrane currents that canceled each other and thus failed to evoke a reliable postsynaptic response. Seemingly indifferent to the tuning of the excitatory synapses, each signal contributed an equal part to the PSTH of the output signal, but the effect of the excitatory synaptic weights was uncovered by the steplike input protocol (Fig. 2F). The broad, graded responses (as opposed to all-or-none) to preferred and nonpreferred stimuli (Fig. 2, G and H) were in accord with experimental results (*5*, *7*, *8*, *23*, *24*) and confirm earlier theoretical studies arguing that sharp tuning is not a necessary feature for a sparse sensory representation (*25*, *26*). The sparsity of the response to each signal was a direct consequence of the detailed balance of correlated excitatory and inhibitory synapses as described above, not of the specificity of the tuning curve.

The self-organizing dynamics of inhibitory plasticity imply that the excitatory-inhibitory balance is maintained, even in the presence of ongoing excitatory plasticity (Fig. 3). Experiments (*7*) in which a stimulus alters the frequency tuning of excitatory input currents to pyramidal neurons in rat primary auditory cortex point in a similar direction: The disrupted cotuning of excitatory and inhibitory input currents (Fig. 3A) prompts a compensatory response that subsequently changes the amplitude of the inhibitory input currents. After 180 min, the cell returns to a cotuned state, albeit with a different preferred frequency (Fig. 3B). When we disturbed the cotuning of a simulated neuron in a similar way (Fig. 3C), inhibitory plasticity rebalanced the excitatory input currents (Fig. 3, D and E) and stabilized the output firing rates of the postsynaptic neurons (Fig. 3F). Quantitative agreement with the rebalancing dynamics observed in the experiment (for both synaptic depression and potentiation) was achieved by adjusting η, ρ_0, and the average firing rate of the inhibitory input neurons.

The learning rule for inhibitory synapses does not rely on a feedforward structure to achieve low firing rates. It simply matches excitatory and inhibitory synapses that show correlated activity. We therefore tested whether inhibitory plasticity was able to stabilize the dynamics of recurrent networks. In simulations of such networks (*13*)

with plastic inhibitory synapses that were initially weak (Fig. 4A), the resulting high firing rates and subsequent increase in inhibitory synaptic strengths caused by the plasticity rule indeed produced globally balanced input currents that led to a self-organized AI network state (Fig. 4B) with firing rates between 3 and 15 Hz.

We wondered whether it was possible to introduce associative memories to the stabilized network by strengthening specific excitatory connections within dedicated groups of neurons. First proposed by Hebb (*27*), such "cell assemblies" aim to provide a physiologically plausible explanation of how groups of neurons form a memory. Groups of highly connected neurons have since been successfully embedded into large spiking networks (*28*) and shown to self-sustain their activity without disrupting the global dynamics of the host network (*13*, *29*, *30*), but the parameter space that guarantees stable performance is narrow and tuning is arduous. The question has been raised how useful such memory attractors can be for long-term memory systems if only one of all stored memories can be active at a time, and potentially remains active for long periods of time, broadcasting the stored information into the network (*29*).

Inhibitory plasticity can solve some of these problems. After two arbitrarily chosen groups of excitatory neurons were turned into Hebbian assemblies by strengthening the excitatory connections within the groups fivefold, the assemblies temporarily fired at high rates and raised the background firing rate across the network (Fig. 4C). The resulting increase of coincident spike pairs caused inhibitory plasticity to increase the inhibitory synapses onto neurons in both assemblies until the global AI state was reestablished (Fig. 4D). After the excitatory and inhibitory inputs onto these neurons had been rebalanced, the firing rates of neurons in the cell assemblies became indistinguishable from the rest of the network, despite the imprinted memory traces in the excitatory synapses. Electrophysiological recordings of neuronal activity would thus not reveal the presence of a synaptic memory trace in this state.

Retrieval of previously quiescent memory items could be achieved by momentarily disrupting the balance within a cell assembly, for example, through additional excitatory input. It was sufficient to drive a small fraction of the cells of one assembly to reactivate all cells of that assembly. Notably, the recall was asynchronous and irregular, as indicated by low correlations between neurons and large variability of the interspike intervals (Fig. 4E). Although we embedded two overlapping assemblies into the network, only one was activated. The rest of the network remained nearly unperturbed in the AI state. Unlike traditional attractor networks, both assemblies could also be activated in unison by driving cells of both memories simultaneously (figs. S4 and S5), and their activity decayed to the background state after the stimulus was turned off.

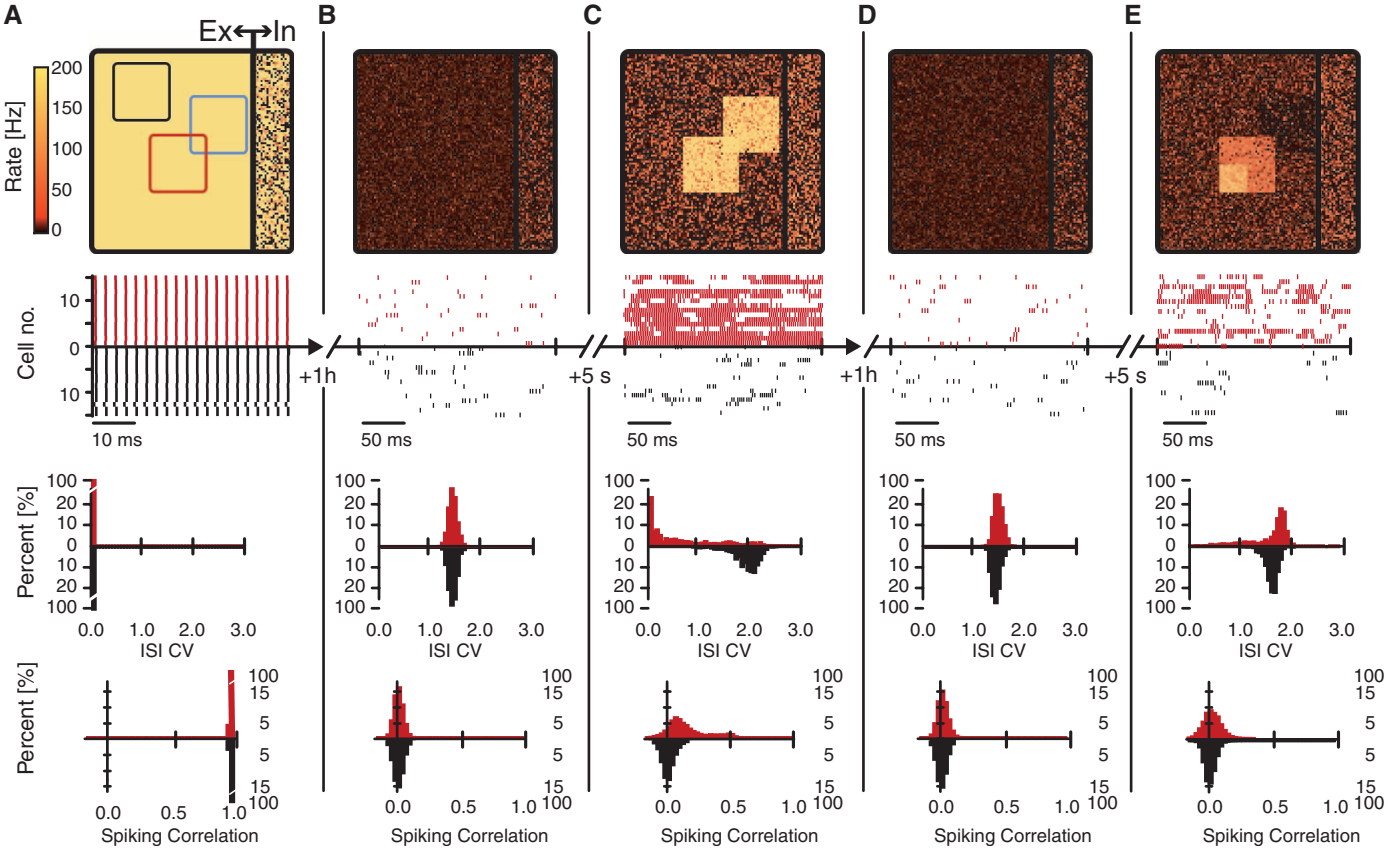

Fig. 4. Inhibitory plasticity in recurrent networks. Five consecutive snapshots of the momentary activity of a network of 10,000 integrate-and-fire cells with inhibitory plasticity. (**A**) Synchronous regular network dynamics with high firing rates at the beginning of the simulation with weak inhibitory synapses. (**B**) Establishment of the AI (steady) state with low firing rates through up-regulation of inhibitory synaptic weights by the synaptic plasticity rule. (**C**) The introduction of two synaptic memory patterns (cell assemblies) by fivefold increased excitatory synaptic weights between neurons outlined in red and blue in (A) leads to high firing rates. (**D**) Recovery of the AI state at low firing rates. (**E**) Memory retrieval through externally driving the lower left quarter of the red cell assembly with an additional excitatory stimulus. Each snapshot (A) to (E) shows (from top to bottom) the following: (i) The momentary (1-s) average firing rate of all neurons on a grid of 100^2 cells and separated into excitatory and inhibitory cells [left and right of the vertical line in (A), respectively]. Three groups of neurons play the role of either a cell assembly (red and blue outlines) or a control group (black outline). (ii) A raster plot of 30 randomly drawn neurons from one (red) cell assembly and the control group, indicated by a red and a black square in the plot above. (iii) The distributions of coefficients of variation of interspike intervals (ISI CVs) recorded from the neurons in the red and black groups. (iv) The distributions of spiking correlations between spike trains from neurons in the same designated groups. For methods and additional statistics, please see SOM.

Our results offer an explanation for how long-term memories can be stably embedded into networks as quiescent and overlapping Hebbian assemblies. Unlike previous studies, our network does not exhibit the behavior of an attractor network, in which activated cell assemblies will compete with each other and the winning pattern often exhibits persistent elevated activity. Instead, the network remains quiet unless the balance of one or more assemblies is modulated in favor of the excitation and returns to the background state when the modulation is turned off. We have shown this effect here by driving a subset of cells with an external stimulus, but there are several conceivable methods to modulate the balance of excitation and inhibition (SOM). The possibility to activate several patterns simultaneously allows the analog combination of patterns into larger composite memories. The capacity of storable and retrievable patterns is likely to depend on complex interactions between dynamics, size, and connectivity of the assemblies and the host network, as well as several other parameters.

We show that a simple, Hebbian plasticity rule on inhibitory synapses leads to robust and self-organized balance of excitation and inhibition that requires virtually no fine-tuning (figs. S6 to S9) and captures an unexpected number of recent experimental findings. The precision of the learned balance depends on the degree of correlation between the excitatory and the inhibitory inputs to the cell, ranging from a global balance in the absence of correlated inputs to a detailed balance for strong correlations. The phenomenon is robust to the shape of the learning rule, as long as it obeys two fundamental requirements: Postsynaptic activity must potentiate activated inhibitory synapses, whereas in the absence of postsynaptic firing inhibitory synapses must decay. Because the balance is self-organized, inhibitory plasticity will most likely maintain balance also in the presence of excitatory plasticity, as long as excitation changes more slowly than inhibition or when excitatory plasticity events are rare.

The mammalian brain hosts a wide variety of inhibitory cell types with different synaptic time scales, response patterns, and morphological target regions. Presumably, these cell types serve different functions, and consequently their synapses may obey several different plasticity rules (*31*). In our simplified model, the dynamics of inhibitory plasticity powerfully contributes to the functional state of cortical architectures and may have a strong impact on cortical coding schemes.

References and Notes

1. N. Brunel, *J. Comput. Neurosci.* **8**, 183 (2000).
2. C. van Vreeswijk, H. Sompolinsky, *Science* **274**, 1724 (1996).
3. M. Tsodyks, T. Sejnowski, *Network Comput. Neural Syst.* **6**, 111 (1995).
4. A. Renart *et al.*, *Science* **327**, 587 (2010).
5. M. Wehr, A. M. Zador, *Nature* **426**, 442 (2003).
6. M. Okun, I. Lampl, *Nat. Neurosci.* **11**, 535 (2008).
7. R. C. Froemke, M. M. Merzenich, C. E. Schreiner, *Nature* **450**, 425 (2007).
8. J. de la Rocha, C. Marchetti, M. Schiff, A. D. Reyes, *J. Neurosci.* **28**, 9151 (2008).
9. B. K. Murphy, K. D. Miller, *Neuron* **61**, 635 (2009).
10. Y. Shu, A. Hasenstaub, D. A. McCormick, *Nature* **423**, 288 (2003).
11. T. P. Vogels, L. F. Abbott, *Nat. Neurosci.* **12**, 483 (2009).
12. W. Gerstner, *Neural Comput.* **12**, 43 (2000).
13. T. P. Vogels, L. F. Abbott, *J. Neurosci.* **25**, 10786 (2005).
14. A. Kumar, S. Rotter, A. Aertsen, *Nat. Rev. Neurosci.* **11**, 615 (2010).
15. J. Cafaro, F. Rieke, *Nature* **468**, 964 (2010).
16. T. Hromádka, M. R. Deweese, A. M. Zador, *PLoS Biol.* **6**, e16 (2008).
17. M. A. Woodin, K. Ganguly, M. M. Poo, *Neuron* **39**, 807 (2003).
18. V. Kilman, M. C. W. van Rossum, G. G. Turrigiano, *J. Neurosci.* **22**, 1328 (2002).
19. K. Hartmann, C. Bruehl, T. Golovko, A. Draguhn, *PLoS One* **3**, e2979 (2008).
20. M. R. DeWeese, M. Wehr, A. M. Zador, *J. Neurosci.* **23**, 7940 (2003).
21. H. Yao, L. Shi, F. Han, H. Gao, Y. Dan, *Nat. Neurosci.* **10**, 772 (2007).
22. S. Crochet, J. F. Poulet, Y. Kremer, C. C. Petersen, *Neuron* **69**, 1160 (2011).
23. L. M. Aitkin, D. J. Anderson, J. F. Brugge, *J. Neurophysiol.* **33**, 421 (1970).
24. I. O. Volkov, A. V. Galazjuk, *Neuroscience* **43**, 307 (1991).
25. P. Seriès, P. E. Latham, A. Pouget, *Nat. Neurosci.* **7**, 1129 (2004).
26. J. Beck, V. R. Bejjanki, A. Pouget, *Neural Comput.* **23**, 1484 (2011).
27. D. Hebb, *The Organization of Behavior; a Neuropsychological Theory* (Wiley-Interscience, New York, 1949).
28. W. Gerstner, R. Ritz, J. L. van Hemmen, *Biol. Cybern.* **69**, 503 (1993).
29. D. J. Amit, N. Brunel, *Cereb. Cortex* **7**, 237 (1997).
30. A. Renart, R. Moreno-Bote, X.-J. Wang, N. Parga, *Neural Comput.* **19**, 1 (2007).
31. M. A. Woodin, A. Maffei, *Inhibitory Synaptic Plasticity* (Springer, New York, 2010).

Acknowledgments: Research was supported by Swiss National Science Foundation grant no. 200020 13287 (Coding Characteristics) and CRSIK0 122697 (Sinergia). Additionally, T.P.V. was supported by the European Community's Seventh Framework Marie Curie International Reintegration grant no. 268436, and H.S. and F.Z. by the European Community's Seventh Framework Program under grant agreement no. 243914 (BRAIN-I-NETS) and 237955 (FACETS-ITN), respectively. C.C. received additional support from a French National Science grant ANR-08-SYSC-005. Thanks to G. Hennequin and A. Woodruff for helpful discussions.

Supporting Online Material

www.sciencemag.org/cgi/content/full/science.1211095/DC1
Materials and Methods
SOM Text
Figs. S1 to S10
Tables S1 and S2
References (*31*–*49*)

13 July 2011; accepted 20 October 2011
Published online 10 November 2011;
10.1126/science.1211095

Autophagy-Dependent Anticancer Immune Responses Induced by Chemotherapeutic Agents in Mice

Mickaël Michaud,[1,2,3]* Isabelle Martins,[1,2,3]* Abdul Qader Sukkurwala,[1,2,3] Sandy Adjemian,[1,2,3] Yuting Ma,[2,3,4,5] Patrizia Pellegatti,[6] Shensi Shen,[1,2,3] Oliver Kepp,[1,2,3] Marie Scoazec,[2,7] Grégoire Mignot,[8,9] Santiago Rello-Varona,[1,2,3] Maximilien Tailler,[1,2,3] Laurie Menger,[1,2,3] Erika Vacchelli,[1,2,3] Lorenzo Galluzzi,[1,2,3] François Ghiringhelli,[8,9] Francesco di Virgilio,[6] Laurence Zitvogel,[2,3,4,5]† Guido Kroemer[1,2,10,11,12]†

Antineoplastic chemotherapies are particularly efficient when they elicit immunogenic cell death, thus provoking an anticancer immune response. Here we demonstrate that autophagy, which is often disabled in cancer, is dispensable for chemotherapy-induced cell death but required for its immunogenicity. In response to chemotherapy, autophagy-competent, but not autophagy-deficient, cancers attracted dendritic cells and T lymphocytes into the tumor bed. Suppression of autophagy inhibited the release of adenosine triphosphate (ATP) from dying tumor cells. Conversely, inhibition of extracellular ATP-degrading enzymes increased pericellular ATP in autophagy-deficient tumors, reestablished the recruitment of immune cells, and restored chemotherapeutic responses but only in immunocompetent hosts. Thus, autophagy is essential for the immunogenic release of ATP from dying cells, and increased extracellular ATP concentrations improve the efficacy of antineoplastic chemotherapies when autophagy is disabled.

Transplantable or primary murine cancers respond to chemotherapy with anthracyclines or oxaliplatin much more efficiently when they grow in syngenic immunocompetent mice than in immunodeficient hosts (*1*, *2*). Similarly, clinical studies indicate that severe lymphopenia negatively affects the chemotherapeutic response of solid cancers (*3*), and immune defects are negative predictors of the response to chemotherapy with anthracyclines or oxaliplatin (*2*, *4*, *5*). Apparently, some successful chemotherapeutics can induce a type of tumor cell stress and death that is immunogenic (*6*–*8*), implying that the patient's dying cancer cells serve as a therapeutic vaccine that stimulates an antitumor immune response, which in turn can control residual cancer cells (*9*, *10*). Immunogenic cell death is characterized by the preapoptotic exposure of calreticulin (CRT) on the cell surface (*11*), postapoptotic release of the chromatin-binding protein high mobility group B1 (HMGB1) (*2*), and secretion of adenosine triphosphate (ATP) (*4*).